CHAPTER 4

ALIGNMENT, COHERENCE AND OPTICAL TESTING

"Every physicist thinks he knows what a photon is,
I spent my life trying to find out what a photon is, and I still don't know"
A Einstein

4.1 ALIGNMENT OF THE INTERFEROMETER

Before the interferometer can be used to perform measurements it must be properly aligned. There are two stages to the alignment procedure - the initial alignment which must be performed whenever the interferometer has been disturbed or a component replaced, and the accurate alignment which is performed periodically or after thermal expansion measurements have been made, when the alignment may have drifted. Although length measurements are possible with the interferometer only approximately aligned, they will be in error due to the Abbe effect: the measurement beam will not be travelling parallel with the length to be measured. The final alignment ensures that the measurement beam travels parallel to the axis of the bar, so minimising this error.

4.1.1 Approximate alignment of interferometer

Depending on how the interferometer has been adjusted or modified, only certain parts of the initial alignment may be necessary.

4.1.1.1 Laser beam launching into fibres

The output beam of each laser is focused via a system of lenses into the core of a single mode optical fibre (see § 3.2.2). This requires careful alignment of the end of the fibre with the focal spot of the microscope objective lens. Firstly, the fibre is positioned by eye close to the focal spot by adjusting the *x-y* positioners. Next, the correct focusing is achieved by careful longitudinal positioning of the fibre ferrule until the laser speckle observed on the mount of the objective lens is at its greatest. The speckle is due to interference between parts of the beam reflected from the surfaces of the ferrule and the

fibre. The size of the speckle is largest when the beam is focused on the ferrule/fibre surface. Finally, the fine adjusters are used to position the fibre on the focal spot and to adjust the focus. The output beam from the fibre is monitored by eye or by the CCD camera in the interferometer until the output beam reaches maximum intensity. The laser launch is then correctly aligned.

4.1.1.2 Component positioning in interferometer

The baseplate of the interferometer has carefully positioned holes for mounting the optical components and their holders. By following the schematic diagram of the interferometer it is simple to fix the components in the right position by bolting them to the baseplate. Exceptions to this are the final 45° mirror, the TV camera and the reference mirror assembly, which all have some degree of freedom in their positioning to allow for adjustment.

4.1.1.3 Fibre positioning in collimator

The optical fibre bundle inside the brass ferrule must be positioned on the axis of the collimator lens. This is achieved by placing an optical flat against the upright surface of the collimator lens mount and adjusting the position of the fibre until the return spot of this autocollimator arrangement is coincident with the source. The lens holder was machined so that the upright is parallel to the rim against which the lens rests. Provided the source is within 1 - 2 mm of the axial focal point, the beam will be sufficiently collimated.

4.1.1.4 Reference mirror alignment

After aligning the collimator, the reference mirror is aligned with the collimated beam. The collimated beam reflects off the collimator mirror and passes through the beamsplitter and is directed by a 45° mirror onto the reference mirror (see figure 3.17). The 45° mirror is adjusted until the beam reflected from the reference mirror is aligned with the interferometer axis. This axis is the path of the axial ray from the source, through the centre of the collimator lens, through the beamsplitter to the reference mirror, and the reverse path. This axis will thus be a normal to the reference mirror surface, once the latter has been aligned.

4.1.1.5 Measurement beam alignment

Having defined the reference axis by adjusting the reference mirror assembly, the other beam reflected at the beamsplitter is the measurement beam which must be aligned with the bar to be measured. This is easily accomplished since the interference fringes will be 'fluffed out' when the reference and measurement beams are co-axially aligned.

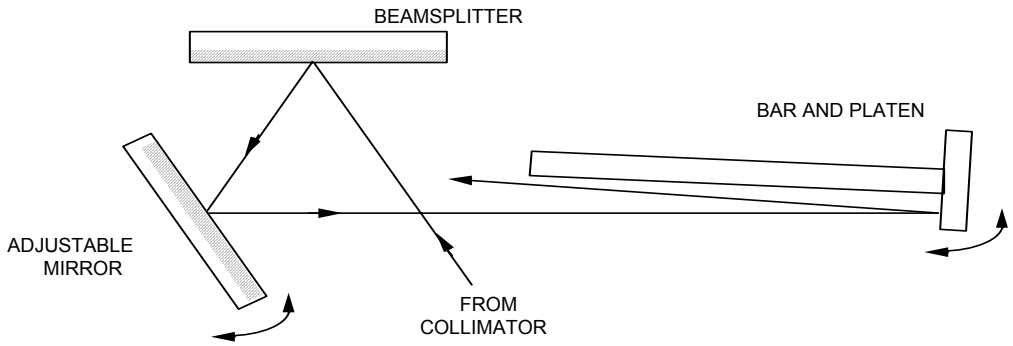

Figure 4.1 *- Aligning the measurement beam with the length bar*

Once the length bar supports have been adjusted so that the bar is approximately aligned with the measurement beam, the mirror in the measurement beam can be used to accurately align the beam with the axis of the bar, as shown in figure 4.1.

4.1.1.6 Alignment of length bars with measurement beam

Having aligned the measurement beam with the axis of one bar, the support carriage is translated until another bar is in the measurement position. The bar supports are adjusted to approximately align the bar with the measurement beam. Any remaining mis-alignment can be removed at the time of measurement by adjusting the measurement beam mirror using the PZTs.

4.1.1.7 Alignment for double-ended interferometry

For double-ended measurements, the interferometer is aligned as follows.

Firstly, the collimator is aligned by using the autocollimation technique, with an optical flat placed against the collimator mount and the fibre position adjusted until the return spot is incident on the fibre end. When the fibre is correctly positioned, the reverse beam will overfill the end of the fibre due to aberrations and diffraction and will thus illuminate the cladding - this can be observed as an increased glow in the fibre. This technique is also suitable for checking the focal positioning.

Next, the reference arm is aligned with the collimated beam by adjusting the tilt of the reference mirror until the return spot is autocollimated onto the end of the fibre.

The bar is placed on the supports, this time positioned at the Airy points of the bar because there is no platen wrung to one end. The measurement beam is adjusted until the fringes are fluffed out on the face of the bar. The axes of the bar, the measurement beam and the reference beam are now aligned, assuming the bar is not out of tolerance on the squareness of the end face with the axis of the bar.

The roof mirror system is inserted. This produces 3 additional return spots at the source corresponding to the beams returned from the front face of the bar and the two oppositely propagating beams which travel around the bar. The return spots of these latter two beams are symmetrically located either side of the spot from the end of the bar, which will be displaced vertically from the source until the vertical tilt of the two mirrors is corrected. Adjustment of the mutual orthogonality of the mirrors directs the two symmetrical spots onto the source.

When the roof mirrors are not orthogonal, the fringes in the background of the image will exhibit a ‘V-shaped’ characteristic, as shown in figure 4.2. This will give rise to extra tilt in the interferogram of the fringes on the rear face of the bar.

When the roof mirrors are adjusted for mutual orthogonality, the tilt of the pair of mirrors is adjusted until the fringes in the background are fluffed out. The interferometer is then completely aligned for double-ended measurements. Any difference in tilt between the two images of the ends of the length bar is due to parallelism errors in the bar. Once the roof mirrors have been set orthogonal with each other, only tilt of the pair of mirrors from the vertical plane will influence the fringes in the image. The imaging of the front face of the bar is unchanged from the single-ended case, except for the magnification.

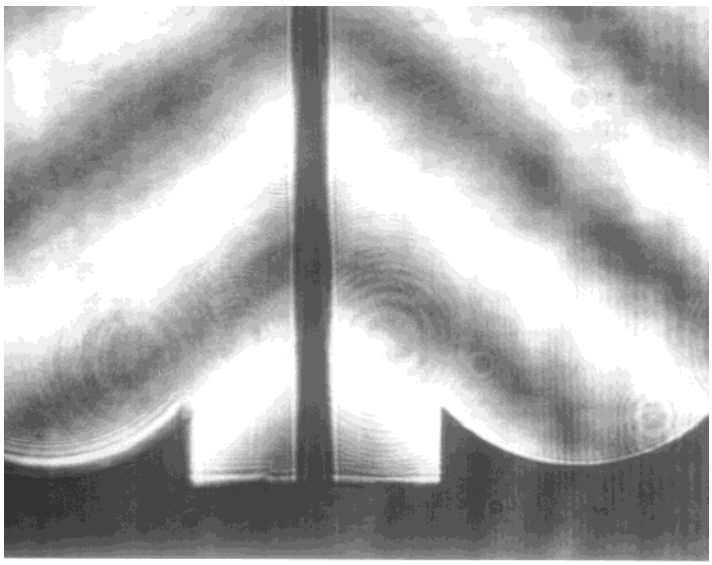

Figure 4.2 *- Incorrect adjustment of roof mirror orthogonality (bar removed for clarity)*

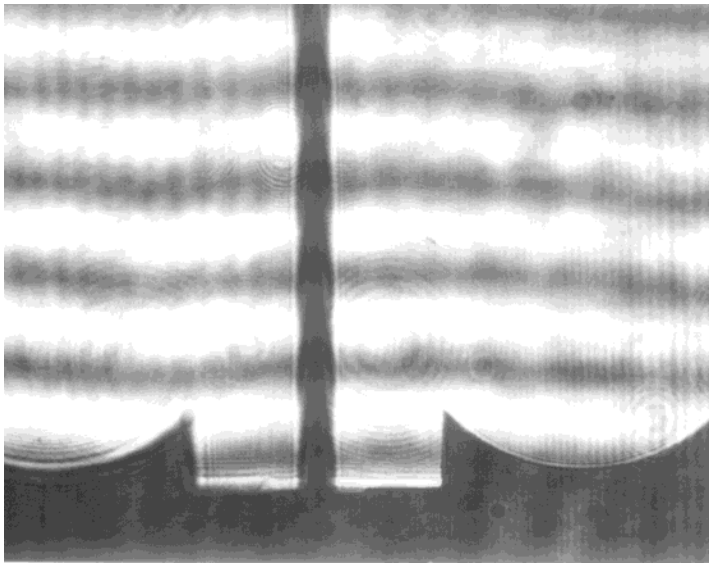

Figure 4.3 *- Correct adjustment of roof mirror orthogonality (bar removed for clarity)*

4.1.2 Accurate alignment of the interferometer

The accuracy of length measurements is critically dependent on the accuracy of alignment of the interferometer. To produce interference fringes visible on the monitor, the reference and measurements beams must be aligned with each other to within approximately 1 arcmin. However, even with fluffed out fringes, the alignment may still be in error and the length measurement inaccurate due to the reference and measurement beams not being aligned with the axis of the bar being measured.

4.1.2.1 Cosine error due to measurement beam mis-alignment

Consider the bar and platen in figure 4.4.

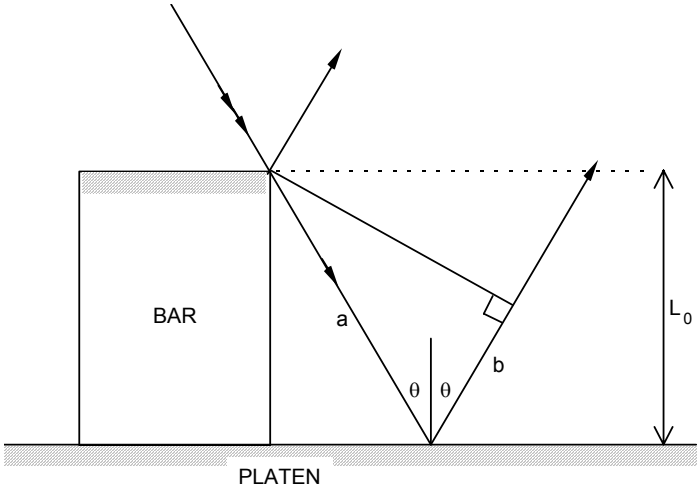

Figure 4.4 *- Cosine error of measurement beam*

The measured length is half the difference in optical path between the two beams, *ΔOPD*.

$$\Delta OPD = a + b$$

$$a = \frac{L_0}{\cos\theta} \quad b = a\cos 2\theta \quad = \quad \frac{L_0 \cos 2\theta}{\cos\theta}$$

$$\therefore \frac{\Delta OPD}{2} \quad = \quad \frac{a+b}{2} \quad = \quad \frac{L_0}{2\cos\theta}[1+\cos 2\theta]$$

$$= \frac{L_0}{\cos\theta}\left[\cos^2\theta\right]$$

$$\text{measured length} = L_0 \cos\theta \qquad (4.1)$$

Hence, unless the measurement beam is aligned with the axis of the bar, the measured length will be subject to a length dependent cosine error. Note, the effect of the end faces of the bar not being perpendicular to the axis of the bar are dealt with in chapter 10 - for now it will be assumed that the bar is a right circular (or rectangular) cylinder.

4.1.2.2 Alignment of the three interferometer axes

There are three axes which must be aligned in the interferometer: the axis of the bar, the reference beam axis and the measurement beam axis. To align all three, a common point of reference must be used: this is the source spot. First, the collimator is aligned using the method described above. Next, the reference arm is aligned with the collimator, followed by alignment of the measurement beam (including the bar). Thus the initial alignment of the reference beam with the collimator is important. A special technique was developed to align this beam.

4.1.2.3 Two-fibre autocollimation technique

The system uses three single-mode optical fibres which have had the buffer coating removed from both ends (see § 3.2.2). At one end the fibres are cemented into a tight bundle. The other end of each of the fibres is individually mounted and polished, see figure 4.5. Each fibre in the bundle can serve two functions; it can act as the light source for the collimator when light from a laser is focused into the fibre core, and secondly the fibre can be used to detect the return spot, when used in an autocollimation arrangement, for which another fibre is used as the light source, see figure 4.6.

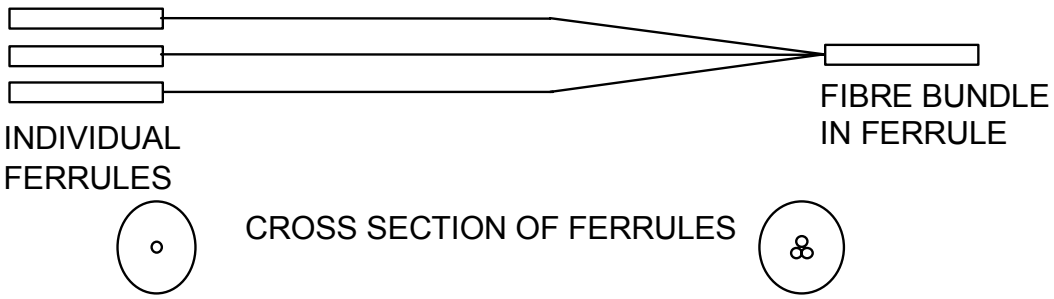

Figure 4.5 *- Three fibre system*

In principle it is possible to use this technique with just one fibre acting as both source and detector though the extra optical components required, such as beamsplitters or couplers, could introduce losses which would make the detection of the return spot more difficult.

When used in the autocollimation arrangement of figure 4.6, the reference mirror of the interferometer is used to reflect the beam back to the source where one of the fibres in the bundle is used to detect the return spot. The fibre bundle is moved in three orthogonal directions and the intensity of the light incident on the detector fibre is monitored using a photodetector placed at the output end of the fibre, after it has been removed from the laser launch optics. When the detected intensity is maximised, the source and detector fibres are symmetrically positioned on either side of the axis of the interferometer, and the principal focus. The off-axis position of the source is then half the separation of the fibres, which is typically 50 μm. This technique aligns the collimator with the reference arm of the interferometer. The expected obliquity error from this system is less than 5.6×10^{-10}, or 0.56 nm in 1 m. After alignment, the detector fibre may be replaced and used to launch a third laser source.

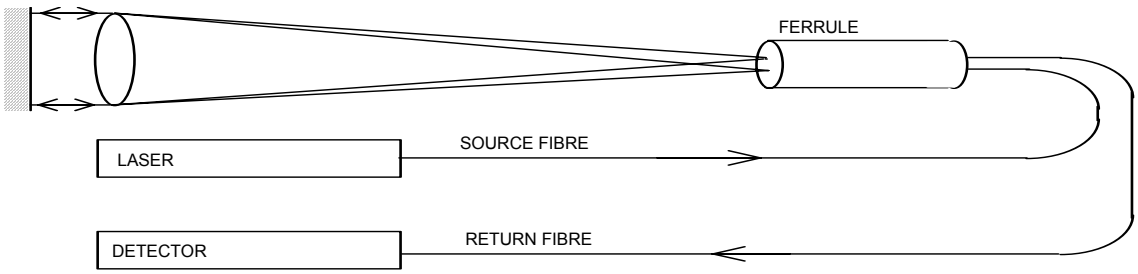

Figure 4.6 *- Autocollimation arrangement*

Evaluation measurements have been made using this system illuminated by the 633 nm red laser. Figure 4.7 shows the peak in the detected intensity as the fibre bundle was positioned radially and axially. These results were repeatable after coarse adjustment over several millimetres of travel.

Assuming the achromatic collimator lens to be diffraction limited, the expected central maximum (Airy disc) of the return spot diffraction pattern should be ~25 μm in diameter [**1**] and should result in a peak of width ~20 μm when a 4 μm diameter fibre is scanned across the moving diffraction pattern, as occurs when the fibre bundle undergoes radial motion. This can be seen in figure 4.7(a). It is thought that the non-symmetrical peaks in the observed data are due to cross-talk from the adjacent fibre which becomes partially illuminated.

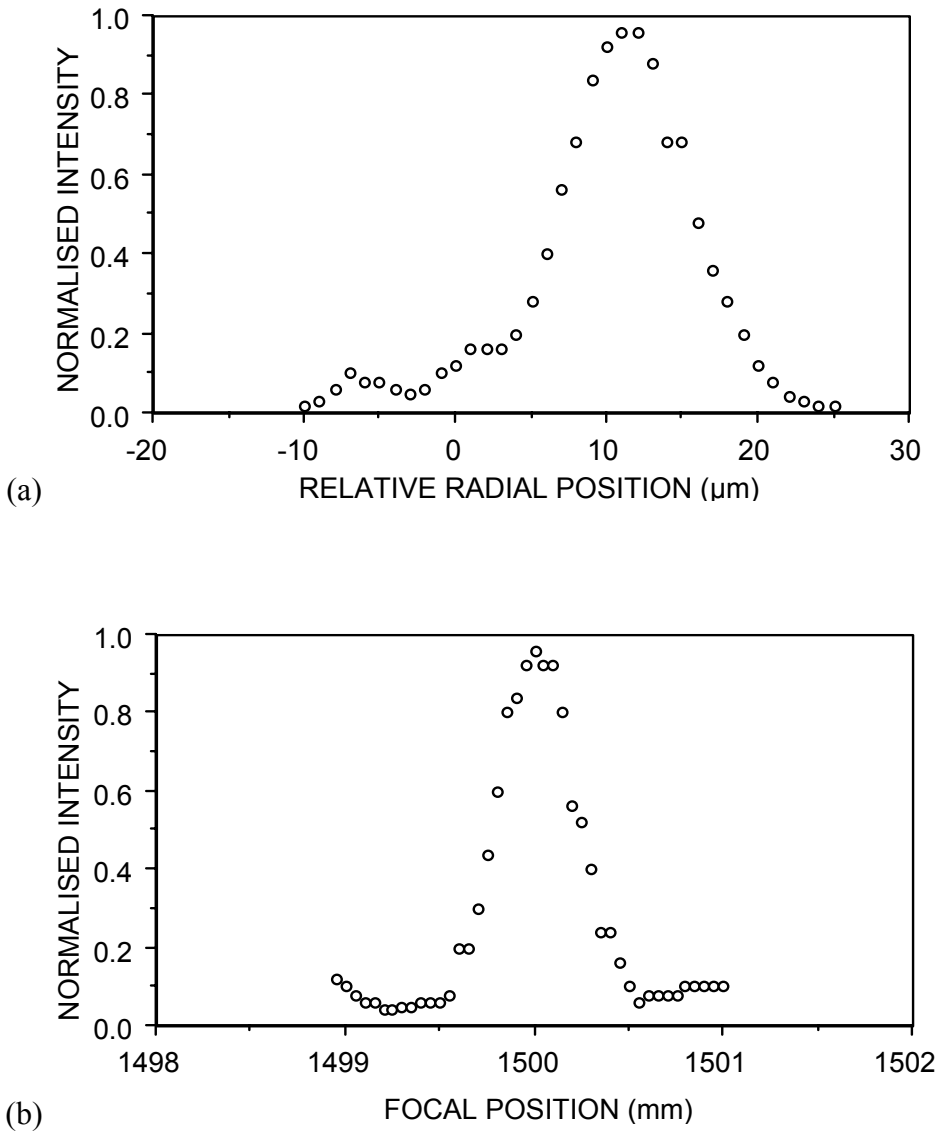

Figure 4.7 *- Detected intensity during (a) radial positioning and (b) axial positioning of the fibre bundle (normalised units)*

When diffraction theory is applied to an un-aberrated circular pupil with defocus it predicts minima in the diffraction pattern, spaced at 1.1 mm along the focal axis. The results shown in figure 4.7(b) are consistent with the theory.

The single-mode fibre system thus provides a simple, efficient, speckle free light source for an interferometer. The autocollimation arrangement using one fibre as a detector allows accurate repositioning of the light source, allowing the collimator beam to be aligned with the interferometer axis, whilst minimising the obliquity effect due to the source. However, with this system the return intensity is low and requires a sensitive detector. It is easier to observe the additional light scattered in the fibre cladding, as described in § 4.1.1.7.

4.1.3 Obliquity effect due to position and size of light source

The light source for the interferometer is the end of an optical fibre, positioned at the focal point of a 100 mm diameter achromat. The source diameter is that of the fibre, which is approximately 4 μm. The fibre is positioned to be nominally on axis, at the correct focal length. However small errors in the positioning can lead to the light source being off axis. This, as well as the finite size of the source contribute errors in the measurement, which can be regarded as obliquity errors, *i.e.* they cause the apparent length of the measured object to be slightly different from the true length. These effects can be removed by using a correction factor. Here, it is shown that the correction factors for the interferometer are very small, due to the design of the collimator, and can be neglected.

When the source is positioned off-axis, the effect can be thought of as causing a small angular deviation, θ, of the measurement path with respect to the object axis. For small θ, there is a correction factor per unit length, C_1, which is $(1-\cos\theta)$, which is approximately $\theta^2/2$. For an aperture of negligible size, at distance s off axis, the correction factor is thus

$$C_1 = \frac{s^2}{2f^2} \tag{4.2}$$

where f is the focal length of the lens. Assuming that the positioning error of the twin-fibre system is ± 50 μm, then for the interferometer, the correction factor for off-axis positioning is

$$C_1 = 5.6 \text{ x} 10^{-10}$$

There is also an obliquity effect due to the finite size of the source [**2**]. This can be considered as the sum of the effects of all infinitesimally small elements which constitute the source. This factor, C_2 , is thus

$$C_2 = \frac{\int_0^{2\pi}\int_0^r \frac{x^2}{2f^2}\, x\, d\phi\, dx}{\int_0^{2\pi}\int_0^r x\, d\phi\, dx}$$

$$C_2 = \frac{r^2}{4f^2} \tag{4.3}$$

For the single mode fibres used, $r \sim 2$ μm, thus $C_2 = 4.4 \text{ x} 10^{-13}$ and is hence negligible. The total obliquity effect is thus $5.6 \text{ x } 10^{-10}$ or a length measurement error of ± 0.56 nm in 1 m.

4.1.3.1 Obliquity effect due to source size - full derivation

Although it is possible to have a correctly aligned interferometer, the size of the source will affect the measurements of phase performed in the interferometer.

Bruce [**2**] considers the extra phase shift introduced to the system due to the source size as an obliquity effect. Consider the circular aperture on axis, in figure 4.8.

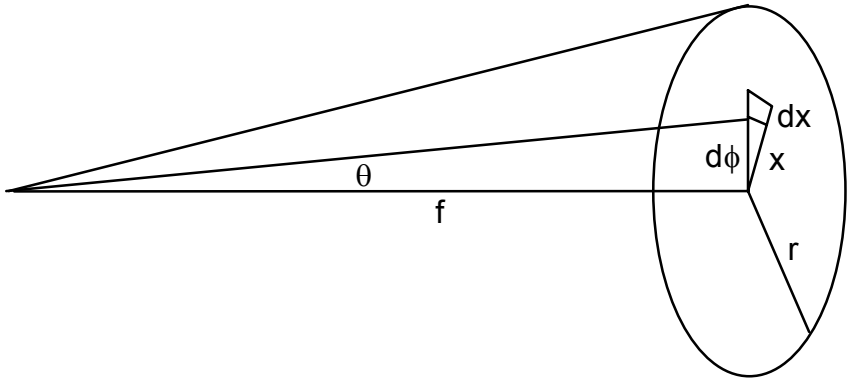

Figure 4.8 *- Obliquity effect due to a circular aperture on axis of interferometer*

The intensity of the interference fringes is given by

$$I = cos^2 K$$

where K = phase difference/2

i.e. $$K = 2\pi L / \lambda$$

where L is the length being measured. For an element of the source at angle θ to the axis, size $d\phi dx$

$$\delta I = \cos^2(K\cos\theta)x\,d\phi\,dx \tag{4.4}$$

For the total effect from the source, integrate over aperture

$$I = \int_0^{2\pi}\int_0^r \cos^2(K\cos\theta)x\,d\phi\,dx$$

Since θ is small, we can approximate cos θ as $1-\frac{x^2}{2f^2}$

$$I = 2\pi \int_0^r \cos^2\left(K - \frac{Kx^2}{2f^2}\right) x\,dx$$

$$= 2\pi \int_0^r \frac{1}{2}\left[\cos\left\{2K\left(1 - \frac{x^2}{2f^2}\right)\right\} + 1\right] x\,dx$$

now substituting

$$u = 2K\left(1 - \frac{x^2}{2f^2}\right)$$

$$du = \frac{2Kx\,dx}{f^2} \tag{4.5}$$

$$I = 2\pi \int \frac{1}{2}[\cos u + 1]\frac{f}{2K}\,du \tag{4.6}$$

$$I = \frac{\pi r^2}{2} - \frac{\pi f^2}{2K}\left\{\sin 2K \cos\frac{Kr^2}{f^2} - \cos 2K \sin\frac{Kr^2}{f^2} - \sin 2K\right\}$$

Substituting for the area of the source A, the obliquity angle θ and the phase factor Δ

$$A = \pi r^2 \qquad \Delta = \frac{K\theta^2}{2} \qquad \theta = \frac{r}{f}$$

$$I = \frac{A}{2}\left[1 + \frac{\sin\Delta}{\Delta}\cos(2K - \Delta)\right] \tag{4.7}$$

Thus the fringes are symmetrical, but displaced by the phase factor Δ from their normal positions. The fringe contrast is also reduced by the factor sinc(Δ).

However for small Δ, approximate $\frac{\sin\Delta}{\Delta} \approx 1$, thus

$$I = \frac{A}{2}[1 + \cos(2K - \Delta]$$

$$= A\cos^2\left(K - \frac{\Delta}{2}\right) \tag{4.8}$$

This equation describes normal $\cos^2$ fringes from an aperture area A, but displaced in phase by $\Delta/2$ compared with those obtained using a point source (on axis).This is the same as the factor C_2 above.

For $0 \le \Delta \le \pi$ the factor $\sin\theta/\theta$ in equation (4.7) is positive and the fringe displacement is given by $\Delta/2$. At $\Delta = m\pi$ (m=1,2,3...) equation (4.7) predicts that the fringes vanish. For the interferometer, with r = 1.8 μm, f = 1.5 m, λ = 633 nm, the first zero of fringe visibility occurs at L = 400 km. Since L < 2 m, the fringes should have good visibility for all sizes of length bar.

Whilst it may not be obvious that a symmetrical source, positioned on axis can produce non-symmetrical shifts in the interference fringes, these effects have been observed by Bruce [**2**] with good agreement (0.001 fringe) between the measured and predicted fringe shifts up to a shift of approximately 0.25 fringe for a 0.78 mm diameter pinhole. The results of these calculations have been confirmed by Thornton [**3**] using a different analysis. It is easier to see the reason for this shift by noting that for any point not on axis, the corresponding beam from this point will travel at an angle to the axis of the bar being measured (obliquity angle) and must therefore measure the length short by the usual cosine factor. Thus all elements of the source lying on an annulus at a particular radius will all contribute an obliquity error of the same sign and magnitude. The results derived above take into account all such annuli.

4.1.4 Collimation check using a shearing plate interferometer

A shearing plate interferometer can be used to translate wavefront curvature into rotation of straight fringes [**4**]. When placed into a properly collimated beam with no aberrations, parallel straight fringes are observed which are parallel to the reference line of the shearing plate. The radius of curvature, R, of an incorrectly collimated beam can be measured using a shearing plate

$$R = \frac{s\delta}{\lambda \sin\theta} \tag{4.9}$$

where s is the shearing distance, δ is the fringe spacing and θ is the fringe rotation from the reference line, measured on the sheared image. Measured values in the collimated beam of the interferometer were s = 7 mm, δ = 7 mm, for λ = 612 nm. A value for θ was estimated to be 0.08 rad (from trigonometry), this places a lower limit on R of 1000 m. The effect of the wavefront curvature on the obliquity is derived as follows.

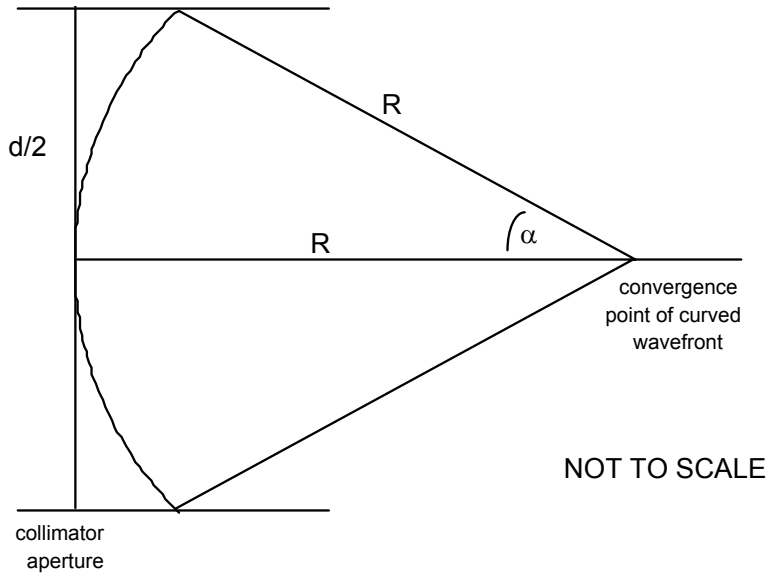

Figure 4.9 *- Convergence of un-collimated wavefront*

$$\alpha \approx \frac{d}{2R} \tag{4.10}$$

For a value for d of 80 mm, $\alpha = 4.0 \times 10^{-5}$. This causes an obliquity effect of magnitude $\alpha^2/2$, which is 1×10^{-9}. The residual wavefront curvature is due to spherical aberration of the achromatic collimator lens, see § 4.1.7.2.

4.1.5 Tilt in the measurement beam

There is an observed change in tilt in the interferogram of approximately + 6 fringes across the image field, when the green laser illuminates the interferometer compared to the red, but only - 1 fringe between the orange and red illuminations (see figure 4.10). A possible source for this differential tilt has been identified, and an estimate of both the magnitude of the tilt and its corresponding obliquity effect are calculated.

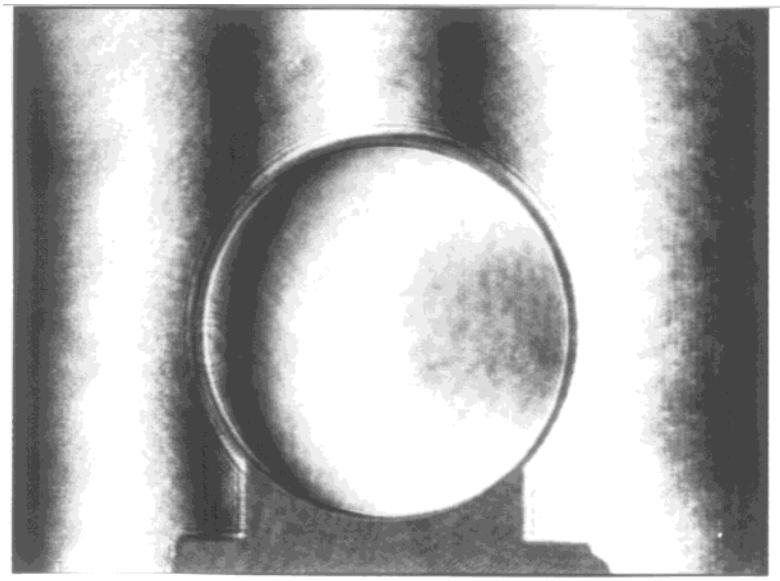

(a) λ = 633 nm

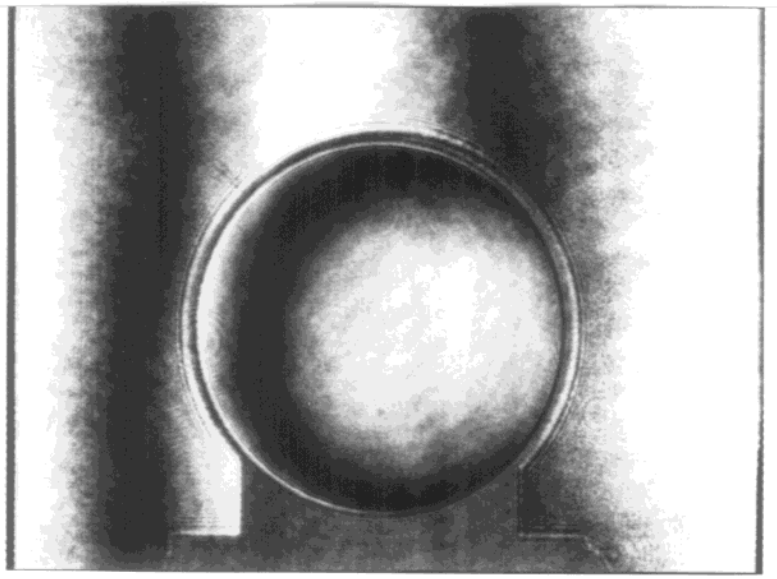

(b) λ = 612 nm

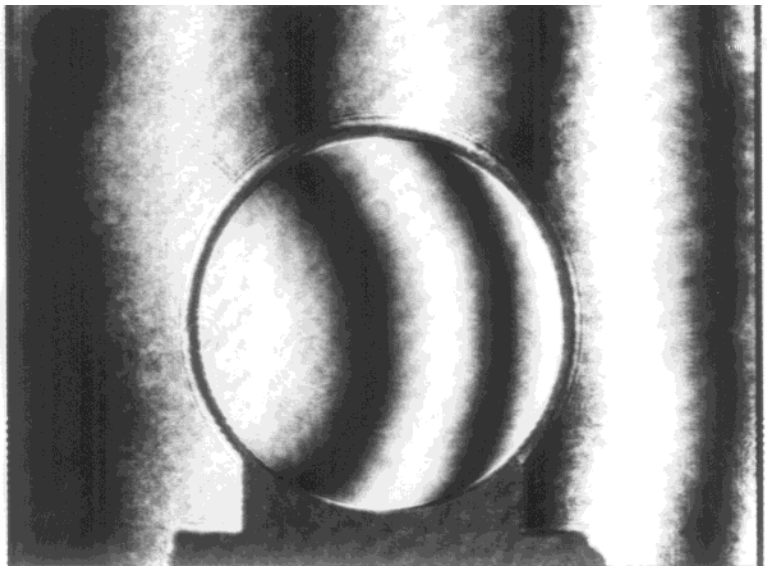

(c) λ = 543 nm

Figure 4.10 *- Difference in tilt between three wavelengths (a) 633 nm, (b) 612 nm, (c) 543 nm*

4.1.5.1 Prismatic dispersion at the beamsplitter

The beamsplitter is wedged at 0.5° to prevent multiple reflections from the non-coated side from interfering with the correct reflection. There is no compensator plate in the interferometer, and thus the beamsplitter acts as a dispersive prism of apex angle γ = 0.5°.

The angular dispersion $d\delta$ for a wavelength change $\delta\lambda$ is given by [**5**]

$$d\delta = \frac{-2\sin(\gamma/2)dn'}{\sqrt{1-n'^2\sin^2(\gamma/2)}} \tag{4.11}$$

For the material of the beamsplitter, fused silica, *dn'* can be found from measurements of *n'(λ)* :

$$n(632.8\text{ nm}) = 1.45702$$
$$n(546.1\text{ nm}) = 1.46008$$

thus *dn'* = 0.00306 for $\delta\lambda$ = 633 - 546 nm, which is approximately the difference between the red and green. This results in

$$d\delta = -2.7\text{x}10^{-5}\text{ rad}$$

This additional tilt produces an extra number of fringes across the image area (width approximately 45 mm) given by

$$\frac{2\times 45\times 10^{-3}\tan(d\delta)}{633\times 10^{-9}}$$

$$\sim 4\text{ fringes}$$

This is only an approximate calculation because values of *dn'* for the actual material of the beamsplitter will be slightly different from those above, however the direction of the additional tilt which is observed is horizontal. This corresponds to the same plane in which the beamsplitter is wedged and is thus a likely candidate for the extra tilt.

4.1.5.2 Methods for compensation of tilt

The tilt could be corrected by use of a wedged compensator, matched to the beamsplitter. However this would be prone to further spurious reflections and

wavefront aberrations and since the obliquity effect of the additional tilt is negligible, it is not worth correcting in the interferometer, as the software removes any tilt from the final phase maps.

An alternative solution would be to use a system of wedged beamsplitter and compensator plate, angled such that the ghost reflections are trapped inside the beamsplitter by successive total internal reflection [**6**] .

4.1.6 Chromatic aberration - tolerance on collimator focal position

Chromatic aberration in the collimator lens leads to a variation in the position of the focal point with respect to wavelength. The variation between the red and green ends of the spectrum is approximately [**7**] *f*/2000 where *f* is the focal length of the collimator achromat, see figure 4.11.

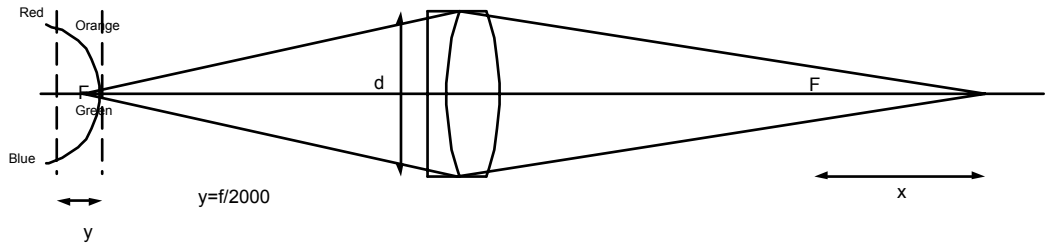

Figure 4.11 *- Chromatic dispersion - effect on focal length of collimator*

For the achromat used in the Primary Length Bar Interferometer, f = 1500 mm. The manufacturer's data states that the variation in focal length between wavelengths 633 nm and 588 nm is 0.47 mm (*i.e.* $y = 0.47$ mm) or *f*/3200. The effect of the afocal positioning of any of the optical fibres can be calculated as follows.

$$xy = f^2$$

and $$y = f/3200$$

hence $$x \sim 4800 \text{ m}$$

Consider one ray of a convergent beam, focal length 4800 m, travelling at an angle θ to the axis of a length bar. The error in the measured length of the bar due to the angle of the beam will be given by

$$\Delta L \approx \frac{L\theta^2}{2}$$

and $$\theta = \frac{d}{2(F+x)}$$

substituting gives $\Delta L = 4.4 \times 10^{-11} L$

If a tolerance is imposed such that $\Delta L < 10^{-9} L$ then it is simple to show that the tolerance on the focus of the collimator is 2.5 mm, which is easily achieved - as shown above, the maximum departure for the achromat used is approximately 0.47 mm.

4.1.7 Optical component quality and spherical aberration

4.1.7.1 Quality of optical components

Measurements of surface quality and subsequent wavefront aberrations of the most important optical components can be found in Appendix B. The majority of the wavefront aberration was found to be spherical aberration.

4.1.7.2 Effect of spherical aberration in collimator

If it is assumed that the wavefront of the interferometer measurement arm contains aberrations, of which the main component is spherical aberration, then the effect of this on the measured length of the length bar can be calculated as follows.

Let the wavefront be of the form $W(x) = ax^4$, where x is a co-ordinate across the wavefront, see figure 4.12.

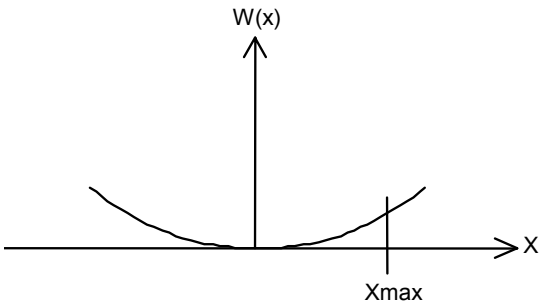

Figure 4.12 *- Spherically aberrated wavefront*

then the angular aberration will be given by $\theta \approx \frac{\partial W}{\partial x}$

$$\therefore \qquad \theta \approx 4ax^3 \tag{4.12}$$

If we now examine the paths travelled by two beams, one un-aberrated, the other aberrated, at an angle θ to the other, where θ is given by the above expression.

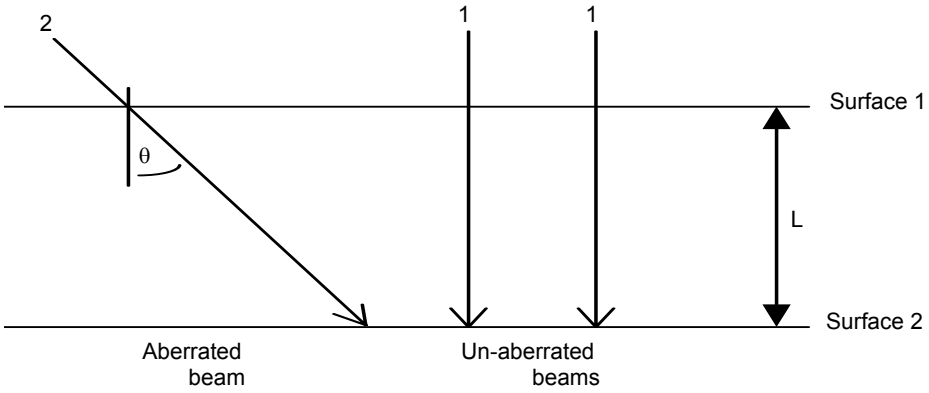

Figure 4.13 *- Interference between two spherically aberrated beams*

These two beams will have phases

$$\phi_1 = \frac{2\pi}{l} 2L \qquad \phi_2 \approx \frac{2\pi}{l} \frac{2L}{\cos q}$$

The phase difference between the two beams will be $\phi_1 - \phi_2$,

$$\phi 1 - \phi 2 = \frac{4\pi L}{l}\left(1 - \frac{1}{\cos q}\right)$$

i.e.

$$\Delta\phi \approx \frac{2\pi L q^2}{l} \tag{4.13}$$

From (4.12) and (4.13),

$$a = \sqrt{\frac{\lambda \Delta \phi}{2\pi L}} \frac{1}{4x^3} \tag{4.14}$$

Substituting $\lambda = 633$ nm, and $x = 40$ mm, the radius of the collimated beam, the path length, $L = 1.5$ m (for a 1.5 m bar), and from the Zygo test measurements of the achromat, $W(x) = 0.15\ \lambda$, a is found to be 0.0371 m^{-3}. Substituting for a gives a value for $\Delta\phi$ of $\Delta\phi = 0.0013$, or 1/770 fringe. This is equal to 0.4 nm, and hence is a small

systematic error. This value is similar to the value of 1 x 10^{-9} obliquity error obtained from the estimate of residual wavefront curvature in § 4.1.4.

4.1.8 Effect of squareness of length bar on measured length

The length of a length bar is defined in BS 5317 :

length. This is defined, with the bar mounted horizontally and referred to the standard reference temperature of 20 °C , as the distance from the centre of one of its faces to a flat surface in wringing contact with the opposite face, measured normal to the surface.

For a bar which is not perfectly square, *i.e.* the end faces are not both perpendicular to the axis of the bar and also parallel with each other, this can lead to differences between the defined and measured lengths of a bar, depending on how the bar is measured.

Consider a non-parallel, singularly non-square length bar, with defined length L_d and another length L_m.

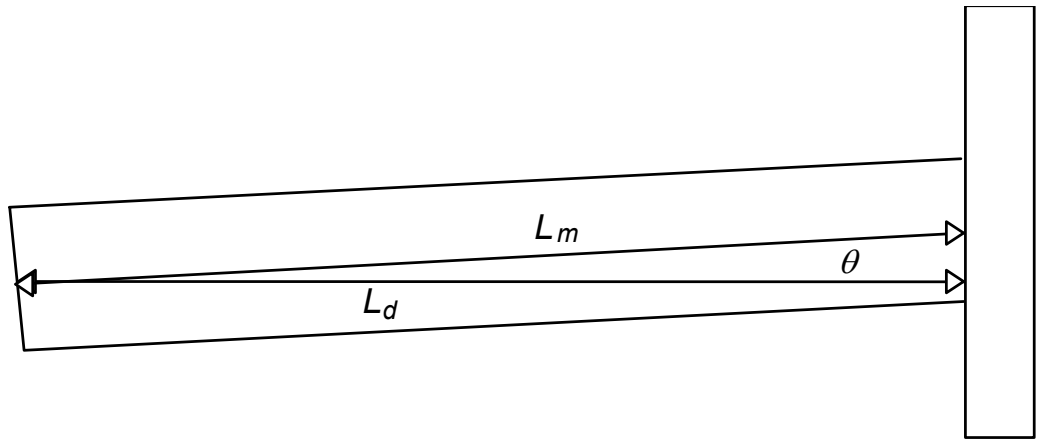

Figure 4.14 *- Non-square, singularly non-parallel length bar*

Because the interferometer is set up with the platen surface normal to the measurement beam (± 2 to 3 fringes of tilt), the length measured by the interferometer is L_d, the defined length of the bar. The NPL Length Bar Machine measures the mechanical central length, L_m, which will be different to the defined length by a factor of size $\cos\theta$, or approximately $\theta^2/2$.

The size of the angle θ will depend on the squareness of the bar. According to the standard, bars should be within 1.2 μm of squareness, for bars up to 400 mm in length, and within 2.5 μm of squareness for longer bars. These values are equivalent to 4 and 8 fringes of squareness error, respectively. By converting these values to angles, it can be

shown that these are equivalent to a length measurement error (for the Length Bar Machine) of 1.6 x 10^{-9} L for bars up to 400 mm, and 6.4 x 10^{-9} L for longer bars.

Note that these errors are for the Length Bar Machine and not for the interferometer, as the latter measures the length of bars in accordance with the definition of length in BS 5317.

4.2 COHERENCE IN THE INTERFEROMETER

The length measurements made in the interferometer are measurements of phase across a relatively large aperture, up to 8 cm in diameter. This requires a high level of both temporal coherence and in the case of double ended interferometry, spatial coherence, as well as high quality optical components with minimum wavefront aberrations.

Temporal coherence is of particular importance as the interferometer has relatively large path lengths and the accuracy required of the length measurements dictates a narrow laser linewidth which is closely linked to temporal coherence. Analogous to the coherence time of the light emitted from the source is the coherence length (as opposed to the spatial coherence measured across the beam pupil). The coherence length must be at least equal to the total path length travelled by the beams before striking the detector array surface.

Although spatial coherence is not so important when using the interferometer in its conventional Twyman-Green arrangement due to the common path, non-sheared optical arrangement, it is however very important when making double-ended measurements (see § 3.3.3). In this arrangement interference is formed between different parts of the beams, some of which have been spatially inverted, *i.e.* sheared. This demands a high degree of spatial coherence between all points in the beam as well as the temporal coherence described above. This can be visualised as a *coherence volume* within which the beam must maintain both temporal and spatial coherence. In wave terms both the magnitude and direction of the wave-vector $\underline{k}$ must be well defined and invariant. For the interferometer the beam must be spatially coherent across the maximum shearing distance of approximately 8 cm and along a path length of up to 7 m, making a coherence volume of 0.035 m^3.

The factors affecting coherence will now be examined and estimates of the spatial coherence and temporal coherence length will be made. For a detailed development of the concept of coherence see Hopkins [**8**,**9**,**10**,**11**].

4.2.1 Temporal coherence

The temporal coherence of a source is a measure of the spread of frequencies (or wavelengths) emitted by the source. A typical quasi-monochromatic source such as a vapour lamp emits frequencies in the range $\omega_0 \pm \varepsilon/2$ of equal amplitude and random phase. This can be illustrated through the use of the *temporal coherence function*, $\gamma(\tau)$.

$$\gamma(\tau) \equiv \frac{\overline{A(t)A^*(t+\tau)}}{\sqrt{\overline{|A(t)|^2}\,\overline{|A(t+\tau)|^2}}} \tag{4.15}$$

where $A(t)$ is the amplitude at time t, $A(t+\tau)$ is the amplitude at time $t+\tau$, and the bar above the symbols represents a mean value over a long interval. For a quasi-monochromatic source γ is unity for small values of τ but then decreases as τ increases. In fact $\gamma(\tau)$ is the Fourier transform of the spectral intensity (Wiener-Khinchine theorem) and is also related to the visibility of interference fringes, given by Michelson's expression

$$V = \frac{I_{\max} - I_{\min}}{I_{\max} + I_{\min}} \tag{4.16}$$

When interference is formed between two beams of equal intensity, with one beam delayed by τ, then $V = |\gamma(\tau)|$.

To obtain good contrast fringes in the interferometer, $\gamma(\tau)$ must be close to unity for τ of the order of 2.3 x 10^{-8} seconds (time taken for beam to travel 7 m) in other words the coherence time of the source, τ_c must be longer than 10^{-8} s. For most standard light sources such as spectral lamps, the coherence time τ_c is approximately 10^{-9} s due mostly to linewidth broadening. There are two main sources of broadening: Doppler broadening and collision broadening.

The effect of Doppler broadening is to spread the line-shape into a Gaussian profile [**12**] with half width

$$\sigma = \omega_0 \sqrt{\frac{k_B T}{mc^2}} \tag{4.17}$$

where k_B is Boltzman's constant, m is the mass of the particle undergoing the transition, T is the temperature of the gas (in K) and ω_0 is the central frequency of the radiation, or in terms of wavelengths

$$\sigma = \lambda_0 \sqrt{\frac{k_B T}{mc^2}} \tag{4.18}$$

As an example, for a standard krypton lamp with λ_0 = 5.6 x 10^{-7} m at 80 K, the half-width is 1.6 x 10^{-13} m, or 3 parts in 10^7.

The effect of collision broadening is much greater than that of Doppler broadening at atmospheric pressure. This arises due to collisions between atoms in the discharge removing coherence between separate emissions. Thus only in the periods between collisions when each atom is travelling freely will there be coherence. However, most vapour lamps operate at a pressure of a few millibars and under these conditions the effect of collision broadening is less than that of Doppler broadening. Overall, it can be seen that vapour lamps do not posses sufficient temporal coherence required for long path length interferometry.

Fortunately light from a laser is much more coherent, particularly light from a stabilised laser. This is due to the natural coherence exhibited by stimulated emission where the phase of the light emitted by an atom is the same as the wave stimulating it to emit. The limiting factor which determines the linewidth arises from the instabilities of the lasing cavity mirrors together with the small amount of spontaneous emission present in the discharge. A typical linewidth for a He-Ne laser, (see § 3.2.1), is 200 MHz (4 x 10^{-7}) decreasing to about 50 kHz for a stabilised laser (1 x 10^{-10}). This is equivalent to a coherence time of 6 x 10^{-6} seconds which is sufficient for the interferometer.

4.2.2 Spatial coherence

Spatial coherence is a function of the source size: if light from different areas of the source arrives at the image plane with different phases, the visibility of the fringes will decrease due to extra destructive interference.

4.2.2.1 An approximate estimate of the spatial coherence

Consider an incoherent source on axis, illuminating a slit of width x. Behind the slit is a screen. Two points on the screen, A and B are separated by a distance Δ.

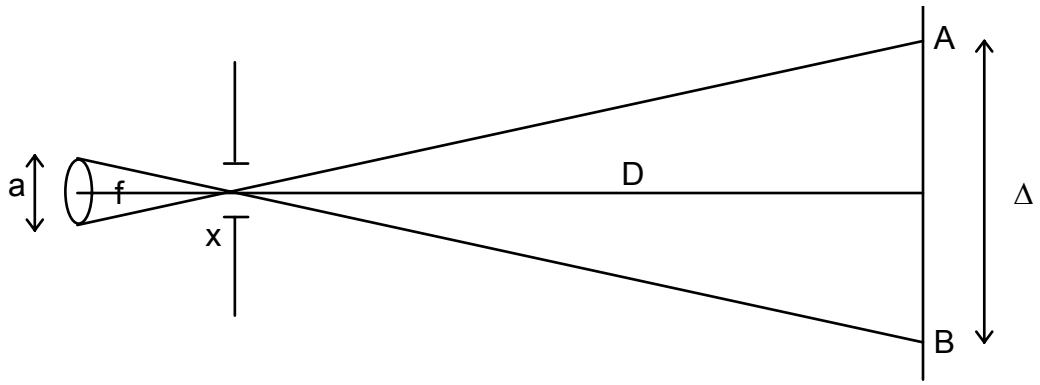

Figure 4.15 *- Coherence of an extended source with slit and screen*

The extended source produces diffraction in the region between *A* and *B*. For an incoherent source, the interference patterns at *A* and *B* are not related as their respective source points are un-correlated and so the two interference patterns will on average cancel each other. If the fringes at *A* and *B* have period ~ $D\lambda/x$ and if the two sets are in anti-phase, then

$$\Delta = \frac{D\lambda}{2x} \tag{4.19}$$

From similar triangles $\Delta = \frac{aD}{f}$

therefore for fringe cancellation $x = \frac{\lambda f}{2a}$

or $x = \frac{\lambda}{2\theta}$ (4.20)

where θ is the angular size of the source.

Thus since the coherence distance in the plane of the pupil is $\lambda f/2a$ the coherence distance is increased by minimising the angular size of the source, as expected. If the source is of fixed size then the remaining option is to increase the source-pupil distance. The source diameter, *a*, is 4 μm thus the spatial coherence distance across the wavefront should be approximately 12 cm.

4.2.2.2 Detailed estimate of the spatial coherence

Just as the temporal coherence function $\gamma(\tau)$ is related via a Fourier transform to the spectral intensity $I(\nu)$, the van Cittert [**13**]-Zernike [**14**] theorem states that the spatial

coherence function $\gamma(r)$ is related to the Fourier transform of the intensity distribution of the source, $I(\theta,\phi)$. This will now be derived (after Lipson & Lipson [**12**]).

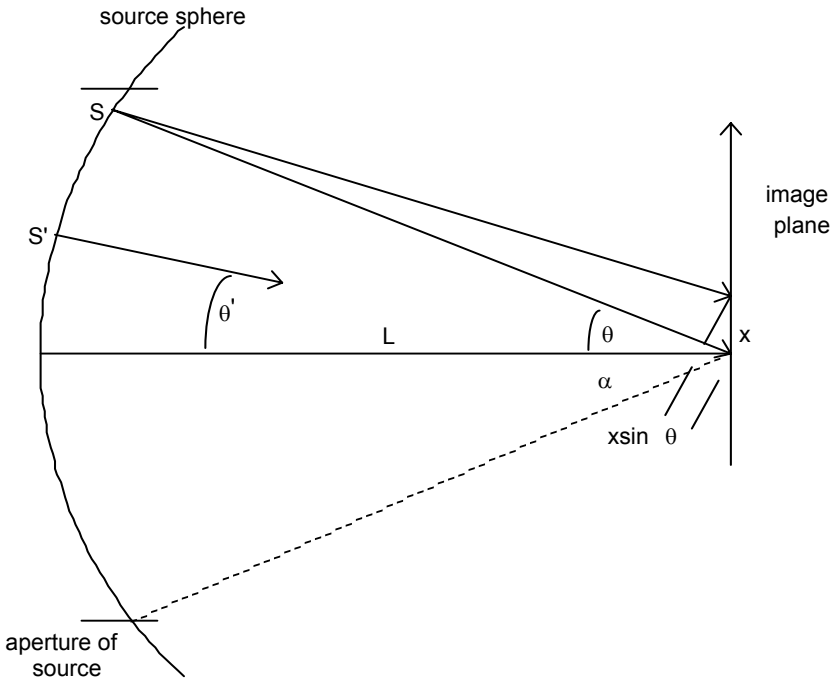

Figure 4.16 *- Source sphere centred on image plane origin*

Consider the source illustrated in figure 4.16. For an incoherent source the amplitudes at different points on the sphere, $g(\theta)$ and $g(\theta')$ are unrelated.

The amplitude in the image plane at $x = 0$ is $A(0)$

$$A(0) = \frac{1}{L}\int g(\theta)e^{-ikSP}d\theta \tag{4.21}$$

and at $x = x$ is $A(x)$

$$A(x) = \frac{1}{L}\int g(\theta)e^{-ik(SP-x\sin\theta)}d\theta \tag{4.22}$$

Defining $c(x) \equiv A(0)A^*(x)$

$$\begin{aligned} c(x) &= \frac{1}{L^2}\int g(\theta)e^{-ikSP}d\theta \int g^*(\theta)e^{-ik(SP-\sin\theta)}d\theta \\ &= \frac{1}{L^2}\int g(\theta)g^*(\theta)e^{-ikx\sin\theta}d\theta \end{aligned} \tag{4.23}$$

Now $$\gamma(x) \equiv \frac{\overline{c(x)}}{\overline{c(0)}} \text{ and } g(\theta)g^*(\theta) = I(\theta) \tag{4.24}$$

$$\overline{c(x)} = \frac{1}{L^2}\int \overline{I(\theta)} e^{-ikx\sin\theta} d\theta$$

For small angles approximate $\sin\theta$ by θ

$$\therefore \quad \gamma(x) = \frac{\int I(\theta) e^{-ikx\theta} d\theta}{\int I(\theta) d\theta} \tag{4.25}$$

i.e. $\gamma(x)$ is the normalised Fourier transform of $\overline{I(\theta)}$.

As an example, if $\overline{I(\theta)}$ is uniform and unity within an incoherent circular source of angular radius α, then $\gamma(x)$ is the normalised Fourier transform of this function which is a Bessel function of the first kind, *i.e.*

$$\gamma(x) = \frac{2J_1(k\alpha x)}{k\alpha x} \tag{4.26}$$

(For an alternative treatment see for example Mandel and Wolf [**15**]).

$\gamma(x)$ falls to zero at $x = 0.61\lambda/\alpha$.

For the interferometer, α = 1.3 x 10^{-6}, thus the first zero of $\gamma(x)$ should be at x = 0.30 m, *i.e.* the wavefront exhibits at least some spatial coherence up to a diameter of 30 cm. This confirms the order of magnitude estimate of 12 cm, to within a factor of 2.5.

The above derivations have assumed an incoherent source. A variant on the van Cittert-Zernike theorem will now be given which does not make this assumption and so will be valid for the coherent source used in the interferometer.

Consider a plane, (ξ,η) containing a source Σ (see figure 4.17). The intensity of an element $d\sigma$ of the source at a point A with co-ordinates (ξ,η) is given by $I(\xi,\eta)$. A second plane (x,y) is separated from the first by a distance R, and contains two points P_1 and P_2.

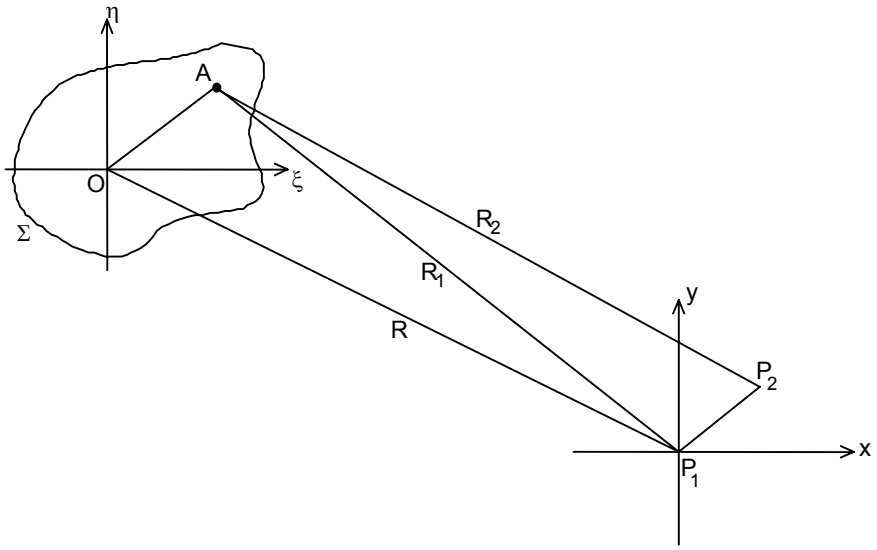

Figure 4.17 *- Coherence between source and image planes separated by R*

Assume that the radiation from Σ is uniform over all angles. The complex amplitudes at P_1 and P_2 produced by an element $d\sigma$ of Σ are u_1 and u_2 respectively.

$$u_1 = \frac{\sqrt{I(\xi,\eta)}}{R_1} e^{-ikR_1} \qquad u_2 = \frac{\sqrt{I(\xi,\eta)}}{R_2} e^{-ikR_2} \qquad k = \frac{2\pi}{\lambda}$$

γ_{12} defined before as $\gamma(x)$ is the complex degree of coherence between P_1 and P_2 and is given by

$$\gamma_{12} = \frac{1}{\sqrt{I_1 I_2}} \int_{\Sigma} \frac{I(\xi,\eta)}{R_1 R_2} e^{ik(R_2 - R_1)} d\sigma \tag{4.27}$$

i.e. the coherence factor between P_2 and P_1 is the same as the complex amplitude at P_2 in the diffraction pattern associated with the aperture Σ with the pattern centred on P_1.

If P_1 is at the origin in the (x,y) plane and P_2 is at (x,y) and A is at (ξ,η) then

$$R_2 - R_1 = \frac{\sqrt{x^2 + y^2}}{R_1 + R_2} - \frac{2}{R_1 + R_2}(x\xi + y\eta) \tag{4.28}$$

For small values of x,y and with a sufficiently large source

$$R_2 - R_1 \approx -\frac{1}{R}(x\xi + y\eta) \tag{4.29}$$

$$\therefore \gamma_{12} = \frac{1}{R_2\sqrt{I_1 I_2}} \int_{\Sigma} I(\xi, \eta) e^{\frac{-ik(x\xi + y\eta)}{R}} d\xi d\eta \tag{4.30}$$

i.e. γ_{12} is the Fourier transform of $I(\xi,\eta)$. This is the same result as the van Cittert-Zernike theorem, except that it holds for incoherent sources. This result is for large apertures only. It will now be developed for small apertures. This will be examined for the case of a circular source, angular radius α, centred on the origin, after Hopkins [**8**].

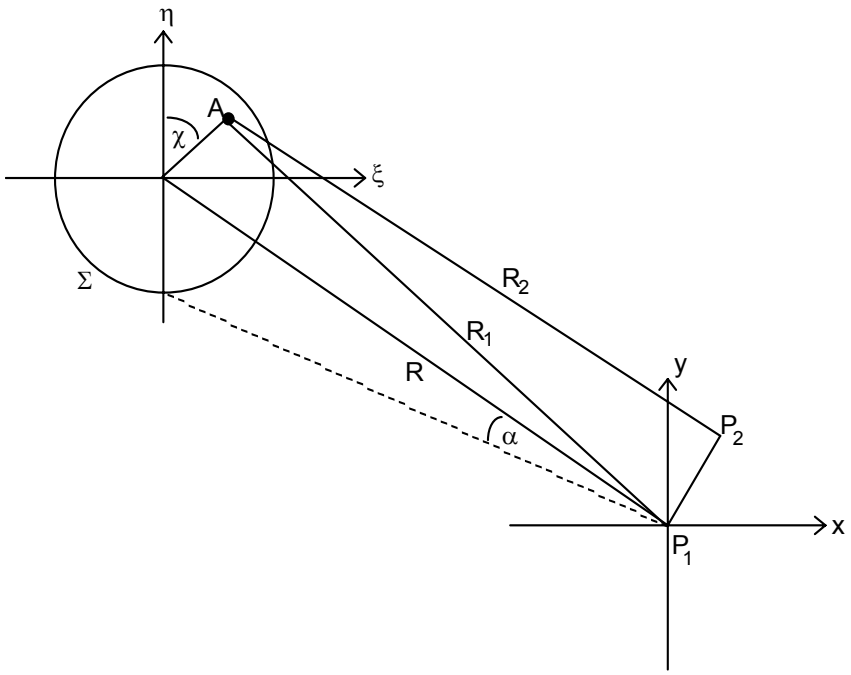

Figure 4.18 *- Coherence from a uniform circular source centred at origin*

Using circular co-ordinates as in figure 4.18

$$r \equiv \frac{\sin\theta}{\sin\alpha} \qquad 0 \le r \le 1$$

From the above definition of γ_{12}, if Σ is small, then $R_2 \sim R_1$

$$\frac{1}{R_1 R_2} \approx \frac{1}{R_1^{\,2}} \tag{4.31}$$

$$\frac{d\sigma}{R_1 R_2} = \frac{R_1 d\chi \, R_1 \tan\theta d\theta}{R_1 R_2} \tag{4.32}$$

$$= \tan\theta d\theta d\chi$$

$$\therefore \quad \frac{d\sigma}{R_1 R_2} = \frac{\sin^2\alpha}{\cos^2\theta} r\,dr\,d\chi \tag{4.33}$$

Now require exponential term of γ_{12} in polar co-ordinates

Define $\rho = \sqrt{x^2 + y^2}$. It can be shown that

$$R_2 - R_1 = \frac{\rho^2}{R_1 + R_2} - \frac{2}{R_1 + R_2}\left(x\xi + y\eta\right) \tag{4.34}$$

Thus the exponential term becomes

$$ik\left\{\frac{\rho^2\cos\theta}{2R} - \rho\sin\theta\cos\left(\chi - \phi\right)\right\} \tag{4.35}$$

Now with $\cos\theta = 1 - \frac{1}{2}\sin^2\theta$ this becomes

$$ik\frac{\rho^2}{2R}\left[1 - \frac{1}{2}\sin^2\theta\right] - ik\rho\sin\theta\cos(\chi - \phi)$$

$$\frac{ik\rho^2}{2R} - \frac{ik\rho^2}{4R}\sin^2\theta - ik\rho\sin\theta\cos(\chi - \phi)$$

Now, correcting a misprint in Hopkins' paper, setting $z = k\rho sin\alpha$ gives

$$\frac{ik\rho^2}{2R} - \frac{i\lambda}{8\pi R}(zr)^2 - izr\cos(\chi - \phi) \tag{4.36}$$

In practice, $z < 10$ and $r < 1$, also $\lambda/R << 1$ and therefore the term in $\frac{\lambda}{8\pi R}(zr)^2$ can be neglected. Thus the exponential term becomes

$$e^{\frac{ik\rho^2}{2R} - izr\cos(\chi - \phi)} \tag{4.37}$$

Substituting this and (4.33) in the expression for γ_{12} gives

$$\gamma_{12} = \frac{1}{\sqrt{I_1 I_2}}\int_0^1\int_0^{2\pi}\frac{I(\xi,\eta)\sin^2\alpha}{\cos^2\theta}e^{\frac{ik\rho^2}{2R}}e^{-izr\cos(\chi-\phi)}r\,dr\,d\chi \tag{4.38}$$

removing terms independent of r and χ gives

$$\gamma_{12} = \frac{\sin^2\alpha}{\sqrt{I_1 I_2}} e^{\frac{ik\rho^2}{2R}} \int_0^1 \int_0^{2\pi} \frac{I(\xi,\eta)}{\cos^2\theta} e^{-izr\cos(\chi-\phi)} r dr d\chi \tag{4.39}$$

If the source is of uniform brightness, $I(\xi,\eta)$ is constant and equal to I, but will decrease by a factor of $\cos^2\theta$ according to the angle θ between the normal to the plane of the source and the propagation direction

$$\gamma_{12} = \frac{I\sin^2\alpha}{\sqrt{I_1 I_2}} e^{\frac{ik\rho^2}{2R}} \int_0^1 e^{-izr\cos(\chi-\phi)} r dr d\chi$$

$$= \frac{I\pi\sin^2\alpha}{\sqrt{I_1 I_2}} e^{\frac{ik\rho^2}{2R}} \frac{2J_1(z)}{z} \tag{4.40}$$

Approximating $I_1 \sim I_2 = I\pi\sin^2\alpha$ gives

$$\gamma_{12} = \frac{2J_1(z)}{z} e^{\frac{ik\rho^2}{2R}} \tag{4.41}$$

This is the same expression as the van Cittert-Zernike theorem except for the factor

$$e^{\frac{ik\rho^2}{2R}}$$

which represents the phase difference of P_2 relative to P_1 due to different optical path lengths from the source to the two points. This is obvious from the limiting case where the source size vanishes

$$\alpha \to 0 \quad , \quad z \to 0 \quad , \quad \frac{2J_1(z)}{z} \to 1$$

$$\gamma_{12} \to e^{\frac{ik\rho^2}{2R}} \tag{4.42}$$

The magnitude of γ_{12} becomes unity and represents a simple phase difference between the two points. Hopkins stated that the modulus of this phase factor was approximately unity except for small α whereas in fact it is always unity and does not depend on α.

After passage through the collimating lens, all such points in the beam should have the same phase, though in the case where α is non-zero, the coherence will vary as the separation of the points, as dictated by γ_{12}.

Figure 4.19 shows the variation of γ_{12} over the two dimensional plane *(x,y)* for the case of the interferometer. Figure 4.20 is a section through this function at $y = 0$ showing the detail. It is common to take a value of γ_{12} of 0.88 as being the cut-off point for coherence (similar to Strehl criterion). From figure 4.21, this occurs at $x = 0.075$ m , for $y = 0$, *i.e.* the diameter of the coherent disc at the entrance pupil is 7.5 cm. Any two points in the double ended system which are sheared by less than 7.5 cm when imaged onto each other will be coherent and produce fringes of suitable contrast.

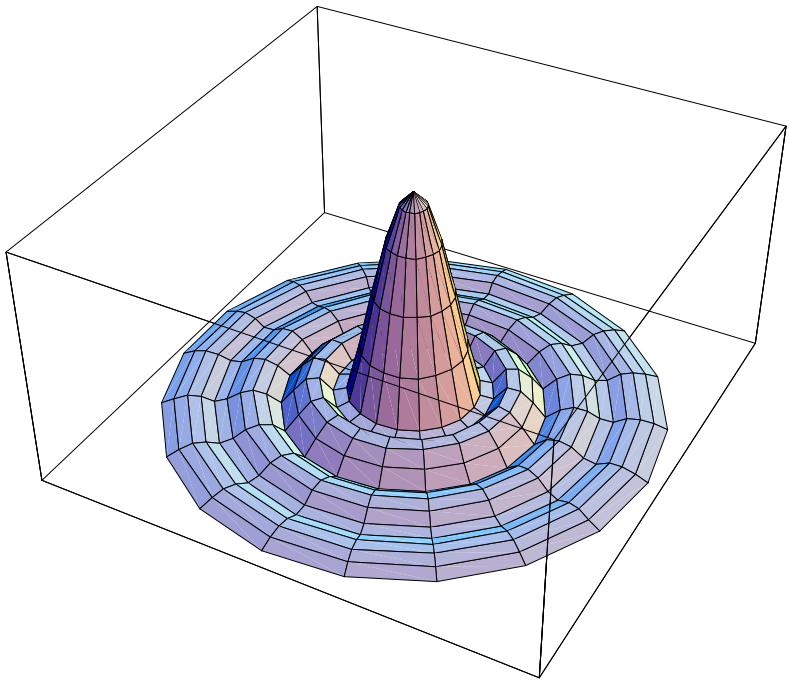

Figure 4.19 *- Variation of coherence over area of image for the Primary Length Bar Interferometer*

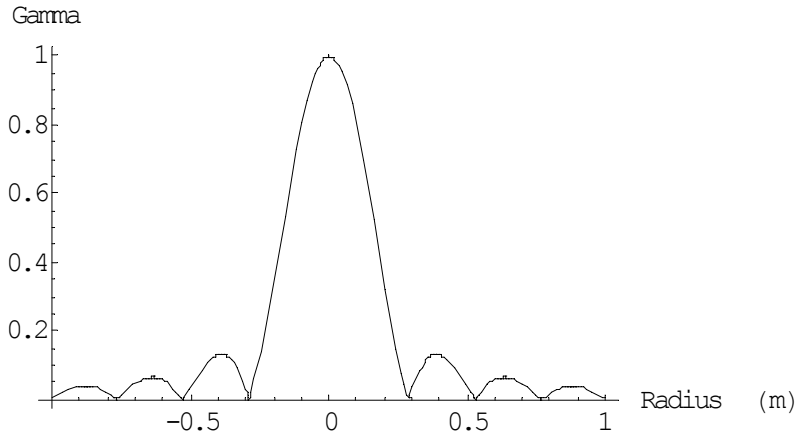

Figure 4.20 *- Section through figure 4.19 showing detail*

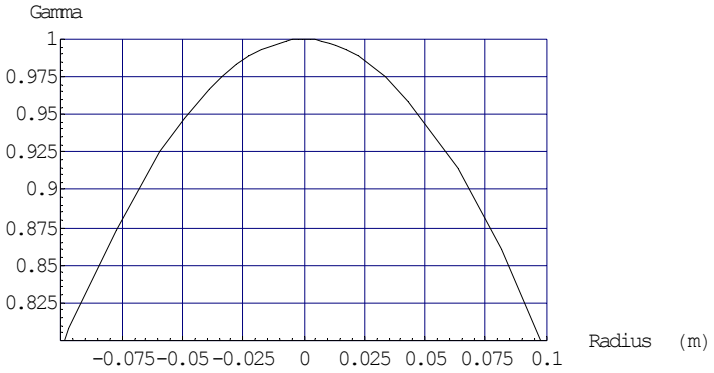

Figure 4.21 *- Region of figure 4.19 about coherence limit of 0.88*

The coherence between points in the beam after the collimating lens may be found using the propagation formulae of Zernike [**14**] or Hopkins [**8**] However if it is assumed that there are no wavefront aberrations due to passage through the collimating lens then, according to Zernike:

"The degree of coherence in a plane illuminated though a lens is the same whether a source of uniform brightness be imaged on the plane or placed directly behind the lens - the phase-changing properties have no influence on the coherence."

And from Hopkins:

$$\Gamma'_{21} = e^{ik[W(x_2,y_2)-W(x_1,y_1)]}\Gamma_{21} \tag{4.43}$$

where (x_1,y_1) and (x_2,y_2) are points in the exit pupil, $W(x,y)$ is the wavefront aberration at point (x,y) in the pupil, T_{21} is the coherence in the entrance pupil and T'_{21} is the coherence in the exit pupil at the corresponding point.

These calculations of the coherence expected in the interferometer are supported by the fact that fringes are observed when the interferometer is operating in double-ended mode, although the fringes corresponding to the sheared beams do have lower contrast compared to the un-sheared fringes. The maximum shearing distance is approximately 8 cm, for which the above calculation predicts a coherence of approximately 0.87, just outside the conventional limit of 0.88. The reduction in fringe contrast can be seen in figure 4.22. The right image of the bar is of the front face, where the image is formed in the same way as for single-ended interferometry. The left image is that of the rear face of the bar, which requires a longer path difference and image shearing. The worst contrast fringes are those in the background which are formed by light which has

travelled twice along the length of the bar and also been sheared. Extra tilt has been added to the fringes for easier viewing.

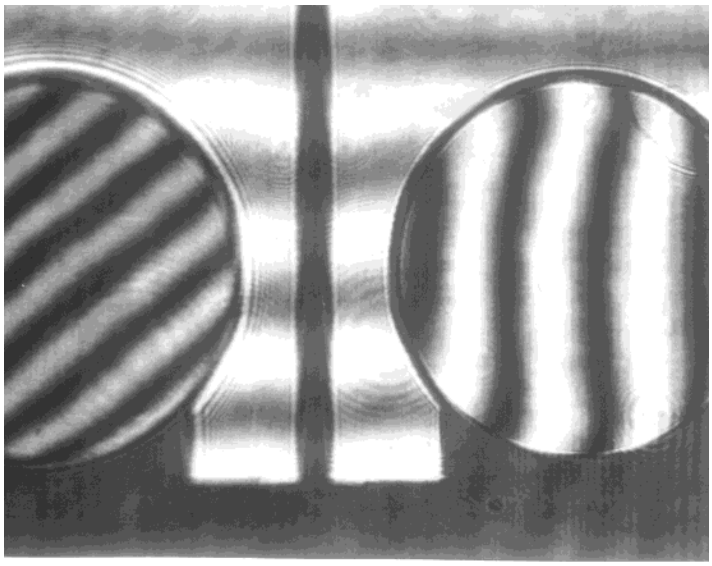

Figure 4.22 *- Double-ended interferogram showing different fringe contrasts*

Note that the effect of tilt due to the wedged beamsplitter is still present in the double-ended interferograms (see figure 4.23). The change in tilt with wavelength is the same as before on the front and rear faces of the bar. The change in tilt of the background fringes is much greater, *e.g.* with the optics adjusted for zero background fringes for the red wavelength, at the orange wavelength there are approximately 8 fringes of tilt across one roof mirror and at the green wavelength there are approximately 11 fringes of tilt (see figure 4.23).

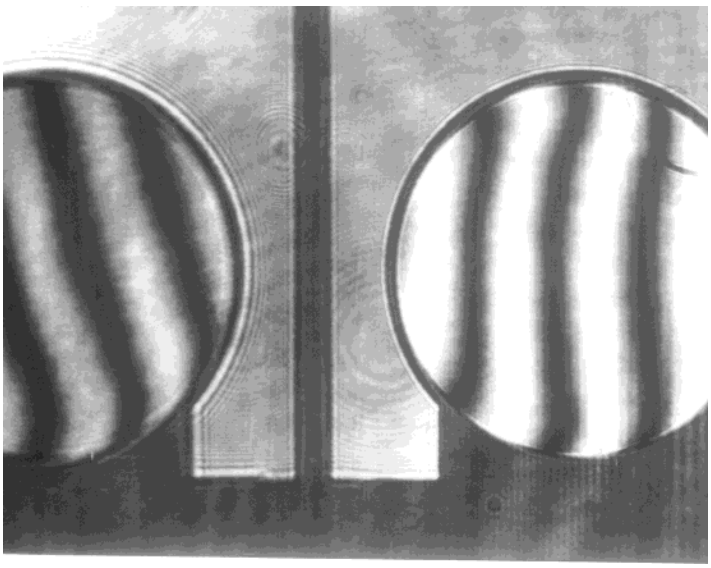

red wavelength

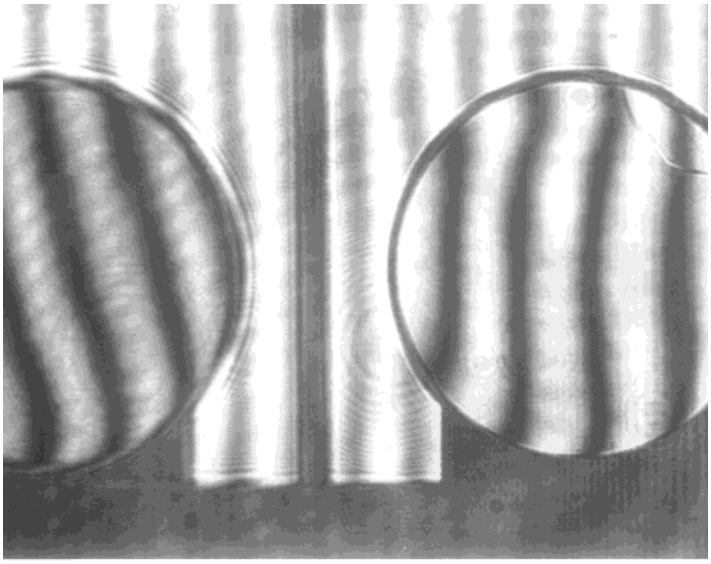

orange wavelength

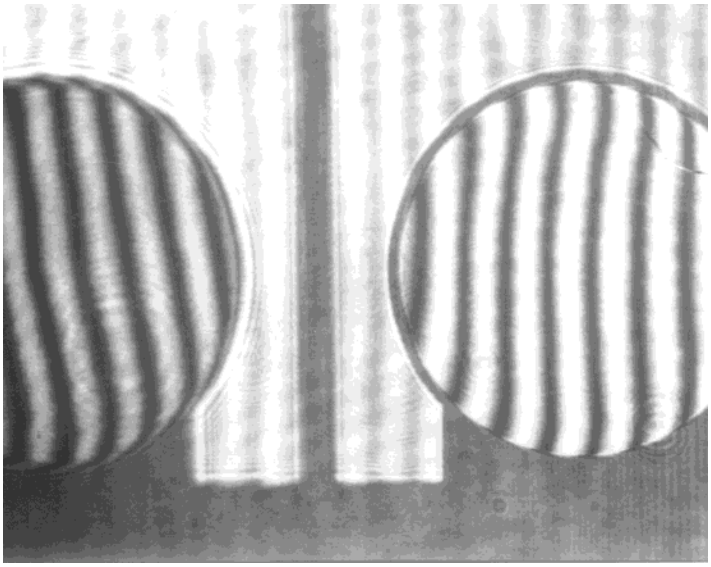

green wavelength

Figure 4.23 *- Double-ended images for three wavelengths, same alignment of optics in all three images*

REFERENCES FOR CHAPTER 4

[**1**] Hecht E *Optics* 2nd Edition (Reading, MA: Addison-Wesley) (1987) 416-421

[**2**] Bruce C F The effects of collimation and oblique incidence in length interferometers *Aust. J. Phys.* **8** (1955) 224-240

[**3**] Thornton B S The effects of collimation and oblique incidence in length interferometers *Aust. J. Phys.* **8** (1955) 241-247

[**4**] Murty M V R K The use of a single plane parallel plate as a lateral shearing interferometer with a visible gas laser source *Appl. Opt.* **3** (1964) 531-534

[**5**] Spindler & Hoyer *Precision Optics* (1989) I1-I2

[**6**] Liepman T W Wedged plate beamsplitter without ghost reflections *Appl. Opt.* **31** (1992) 5905 - 5906

[**7**] Welford W T *Aberrations of Optical Systems* (Bristol: Adam Hilger) (1991) 199

[**8**] Hopkins H H The concept of partial coherence in optics *Proc. Roy. Soc.* **A208** (1951) 263-277

[**9**] Hopkins H H On the diffraction theory of optical images *Proc. Roy. Soc.* **A217** (1953) 408-432

[**10**] Hopkins H H Interferometric methods for the study of diffraction images *Opt. Acta*. **2** (1955) 23-29

[**11**] Hopkins H H Applications of coherence theory in microscopy and interferometry *J. Opt. Soc. Am.* **47** (1957) 508-526

[**12**] Lipson & Lipson *Optical Physics* 2nd Edition (Cambridge: CUP) (1981)

[**13**] van Cittert P H Die Wahrscheinliche Schwingungsverteilung in einer von einer Lichtquelle direkt oder mittels einer Linse Beleuchteten *Physica* **1** (1934) 201-210

[**14**] Zernike F The concept of degree of coherence and its application to optical problems *Physica* **5** (1938) 785-795

[**15**] Mandel L & Wolf E Coherence properties of optical fields *Rev. Mod. Phys.* **37** (1965) 231-287